Inorganic Chemistry

pubs.acs.org/IC

Article

Bioinspired CNP Iron(II) Pincers Relevant to [Fe]-Hydrogenase (Hmd): Effect of Dicarbonyl versus Monocarbonyl Motifs in H_2 Activation and Transfer Hydrogenation

Zhu-Lin Xie, Wenrui Chai, Spencer A. Kerns, Graeme A. Henkelman, and Michael J. Rose*

Cite This: https://dx.doi.org/10.1021/acs.inorgchem.9b03476

Read Online

ABSTRACT: A set of bioinspired carbamoyl CNP pincer complexes are reported that are relevant to [Fe]-hydrogenase (Hmd). The *dicarbonyl* species $[(C^{NH}N^{NH}P^{R2})Fe(CO)_2I]$ [R = Ph, **1**; R = ^{i}Pr, **2**] undergoes ligand deprotonation, resulting in the dearomatized complexes of formulas $[(C^{NH}N^{N=}P^{R2})Fe(CO)_2]$ (**5** and **6**). The crystal structure and $^1H\{^{31}P\}$ NMR spectroscopy of the iodide-bound dearomatized species $[Na(18\text{-crown-}6)][(C^{NH}N^{N=}P^{Ph2})Fe(CO)_2I]$ (**7**) showed that the deprotonated moiety was the phosphoramine N(H) linkage. Separately, the *monocarbonyl* complexes $[(C^{NH}N^{NH}P^{R2})Fe(CO)(MeCN)_2](BF_4)$ (**8** and **9**) synthesized, as well as deprotonated and dearomatized in similar fashion. Reactivity studies revealed that the parent *dicarbonyl* complexes require more forceful conditions for H_2 activation, compared with the *monocarbonyl* complexes. The ligand backbone was not found to participate in H_2 activation and H_2 → hydride transfer to an organic substrate was not observed in either case. Density functional theory calculations revealed that the higher reactivity of the *monocarbonyl* complex in H_2 splitting could be attributed to its higher affinity for H_2. This behavior is attributed to two key points related to the requisite $d_\pi(Fe) \rightarrow \sigma^*(H_2)$ back-bonding interaction in a conventional M−H_2 Kubas interaction: (i) generally, the weaker π donor capacity of the dicarbonyls, and (ii) specifically, the detrimental effect of a strongly π acidic CO ligand (versus weakly π acidic MeCN ligand) trans to the H_2 activation site. The higher reactivity of the *monocarbonyl* complex is also evidenced by the catalytic transfer hydrogenation by *monocarbonyl* **8**, whereas *dicarbonyl* **1** was ineffective. Overall, the results suggest that Nature uses the dicarbonyl motif in [Fe]-hydrogenase to *diminish* the interaction between the Fe center and dihydrogen, thereby preventing premature H_2 activation prior to substrate (H_4MPT^+) binding and any resulting nonspecific hydride transfer reactivity.

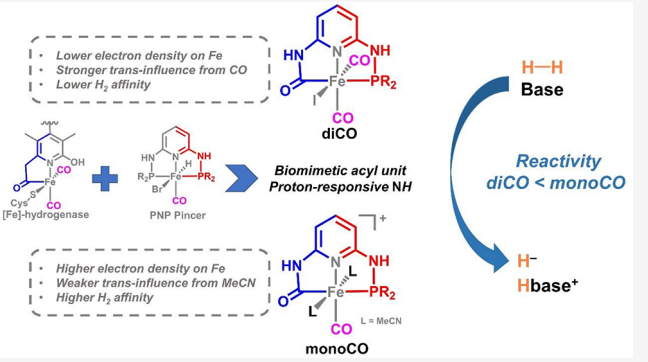

INTRODUCTION

As the availability and environmental cost of fossil fuels make their extraction increasingly difficult, the world's energy sources are slowly shifting from traditional energies to renewable energies.[1−3] One promising alternative renewable energy source is dihydrogen (H_2), which has many advantages: zero carbon emission, high mass energy density (120 MJ/kg), and high energy efficiency in combustion.[4] Despite the benefits of dihydrogen, its generation limits its applications, because 95% of H_2 production is derived from carbon-intensive methods, such as steam reforming and water−gas shift.[5] Although methods such as biomass fermentation and direct water-splitting have drawn substantial attention from researchers, the efficiency of H_2 generation remains an issue.[6] This motivates the development of more-efficient catalysts for both H_2 generation and utilization derived from Earth-abundant elements.

In Nature, H_2 is both generated and utilized by hydrogenases. To date, three types of hydrogenases have been discovered: [NiFe]-hydrogenase, [FeFe]-hydrogenase, and [Fe]-hydrogenase.[7] In contrast to the thorough understanding of the bimetallic hydrogenases, studies of [Fe]-hydrogenase remain relatively nascent. The enzyme [Fe]-hydrogenase catalyzes a non-redox hydride transfer from H_2 to the substrate methenyl-tetrahydromethanopterin (H_4MPT^+), which serves as a C_1 carrier in methanogenic carbon dioxide (CO_2) reduction (see Scheme 1).[7−9] This metalloenzyme (also called Hmd: H_2-forming H_4methylene-PT dehydrogenase) plays an obligate role in "nickel-free" CO_2 → CH_4 metabolism in the absence of bioavailable nickel (and thereby, [NiFe] hydrogenase).[7−9] The active site of [Fe]-hydrogenase (FeGP cofactor) exhibits a unique array of nonproteinaceous ligands (except for Cys_{176}), including a *cis*-dicarbonyl motif, a bidentate pyridone-acyl unit

Received: December 4, 2019

Scheme 1. Reaction of Methenyl-H_4MPT$^+$ to Methylene-H_4MPT by [Fe]-Hydrogenase and the Structure of FeGP Cofactor

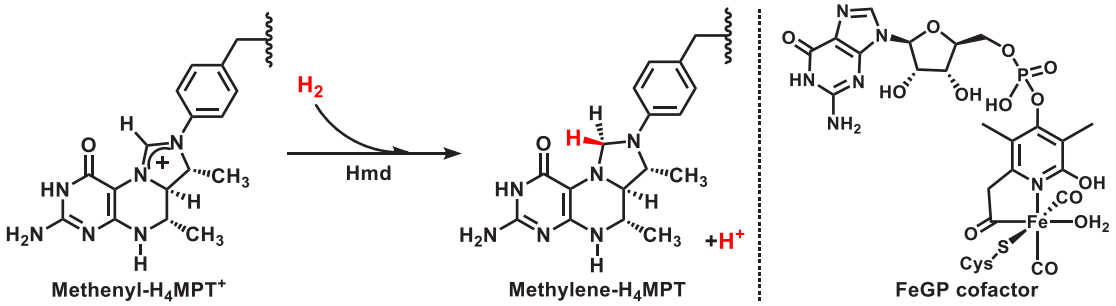

that presents a unique (to biology) organometallic Fe−C bond, and a substrate binding site occupied by a weakly bound H_2O in the resting state.[10,11]

Computational studies of [Fe]-hydrogenase have evaluated several plausible mechanisms of H_2 splitting. Hall and co-workers[12] performed density functional theory (DFT) calculations on a simplified active site. This study suggested that the active site binds and activates H_2 in a stepwise fashion without the participation of substrate (H_4MPT^+). The coordination site *trans* to the acyl unit is ideal for binding and cleavage of H_2, as it requires the minimum structural change on the ligand backbone during the catalytic circle. The main pathway of H_2 heterolytic splitting utilized metal−ligand bifunction between iron(II) and the (deprotonated) pyridone-oxygen. The resulting iron-hydride intermediate was calculated along the reaction trajectory and provides hydride transfer to H_4MPT^+ with an accessible activation barrier (15.2 kcal/mol). In 2014, Reiher and co-workers[13] reported a theoretical study based on the full protein structure using a multiscale modeling method (quantum mechanics/molecular mechanics (QM/MM)). In contrast to the previously proposed mechanism, Reiher suggested that the protein scaffold that harbors the FeGP cofactor provides the necessary conformation change for the substrate to approach the active site. As such, the coordinated H_2 can be cleaved by the orbital push−pull effect between the pyridone oxygen and the cationic carbon on the substrate imidazolium ring (ΔE_a = 1.0 kcal/mol). As a result, no formal iron-hydride intermediate was implicated.

In a *nonbiomimetic* synthetic system (Scheme 2), Kirchner[14] reported $P^{NH}N^{NH}P$ iron(II) carbonyl complexes, in which the dicarbonyl complex $[(P^{NH}N^{=N}P)Fe(CO)_2]^+$ cleaves H_2 via a metal−ligand bifunctional mechanism, leading to the hydride complex $[(P^{NH}N^{NH}P)Fe(CO)_2(H)]$ (**a**; L = CO). Later, the same group[15] reported that the monocarbonyl complexes $[(P^{NH}N^{NH}P)Fe(CO)(L)(H)]$ (**a**), with labile ligands (L = Br^-, MeCN, BH_4^-) *trans* to the hydride, are efficient catalysts for hydrogenation of ketones and aldehydes to alcohols. In parallel, methylene-spaced PNP iron monocarbonyl complexes (**b**) developed by Milstein have been applied to hydrogenation of CO_2,[16] ketones[17,18] and trifluoroacetic esters[19] with high efficiency. Relatedly, Hu synthesized a third type of PNP iron complex with an oxygen spacer (**c**) that performed methanol-assisted H/D scrambling and hydrogenation and transfer hydrogenation of aldehydes.[20]

Returning to [Fe]-hydrogenase, the mechanisms proposed in DFT calculations warrant experimental investigation by synthesizing model complexes that faithfully mimic the active site. In this vein, Hu[21−23] and (separately) Pickett[24,25] reported a series structural models containing acyl-methylpyridine (**d**, **e**, and **f**) and "carbamoyl"-pyridine ligands (**g**, **h**, and **i**) (Scheme 2). Later, Hu and Shima[26] reported semisynthetic [Fe]-hydrogenases comprised of apoenzyme reconstituted with pyridine- and pyridinol-containing iron complexes. The construct containing 2-hydroxypyridine (conjugate base: pyridone) exhibited detectable turnover frequencies in the forward and reverse reactions of [Fe]-hydrogenase (2 s^{-1} and 1 s^{-1}, respectively). In contrast, the methoxy analogue did not exhibit any catalytic activity above the detection limit. These results revealed the importance of the 2-hydroxy group—presumably as a pendant base that accepts H^+ during H_2 cleavage. The above reports also supported the second mechanism[13] (proposed by QM/MM) in which the protein scaffold is imperative for the catalytic activity.

Our own foray into this area commenced with the development of carbamoyl-pyridine-thioether (CNS) iron carbonyl complexes (Scheme 2).[27] The dicarbonyl bromide species (**j**) bears a tridentate ligand backbone with C, N, S ligating in meridional mode. With this pincer-type mimic, we observed the first Fe−H species relevant to [Fe]-hydrogenase by treating the bromide salt with $KHBEt_3$. However, the thermal instability of the hydride species resulted in the isolation of desulfurized complex (**k**) with a $[Fe_2S^{Me}_2]$ core derived from C−S bond cleavage. Similarly, treating the bromide complex with a strong base, KO^{t}Bu, led to C−S bond cleavage, forming a CNC pentacoordinate Fe complex (**l**). It is likely that KO^{t}Bu generated a putative deprotonated carbamoyl intermediate $[(^{O=}C^{N=}NS^{Me})Fe(CO)_2]$, which triggered the desulfurization process. We have also reported model systems based on an "anthracene scaffold".[28,29] The anthracene scaffold tethers the C,N,S donors to provide the facial motif found in the active site. Reactivity studies showed that the complexes $[(Anth{\cdot}C^{NH}NS^{Me})Fe(CO)_2(THF)]^+$ (**m**) and $[(Anth{\cdot}C^{NH}NS)Fe(CO)_2(PhCN)]$ (**n**) are functional for H_2 activation.

In this work, we report a bioinspired "hybrid" system that contains elements of both the biological motif (iron-acyl bonding) and proven catalytic platforms (phosphine pincer), while maintaining a pendant base at the pyridine *ortho* position. We aspired to "connect" the reactivity patterns of purely bioinspired complexes (*fac*-CNS chelates) with purely synthetic systems (*mer*-PNP chelates), as well as to clearly understand the discrepancy between the *dicarbonyl* motif found in [Fe]-hydrogenase and the *monocarbonyl* motif found in synthetic phosphine catalysts. Herein, we report a bioinspired CNP pincer complex with a biomimetic pendant base and carbamoyl group. The experimental and computational studies were performed regarding the synthesis, dearomatization, H_2 activation, and transfer hydrogenation within this model system.

https://dx.doi.org/10.1021/acs.inorgchem.9b03476
Inorg. Chem. XXXX, XXX, XXX−XXX

Scheme 2. Non-biomimetic and Biomimetic Iron Carbonyls for H_2 Reactivity and Hydride Transfer: (i) PNP Pincer Iron Carbonyls,[14−20] (ii) Acyl-Methylpyridine Mimics,[21−23] (iii) Carbamoyl-Pyridine Mimics,[24,25] (iv) Carbamoyl-Pyridine-Thioether Mimics,[27] (v) Scaffold-Based Functional Mimics,[28,29] and (vi) Structures Obtained in This Work

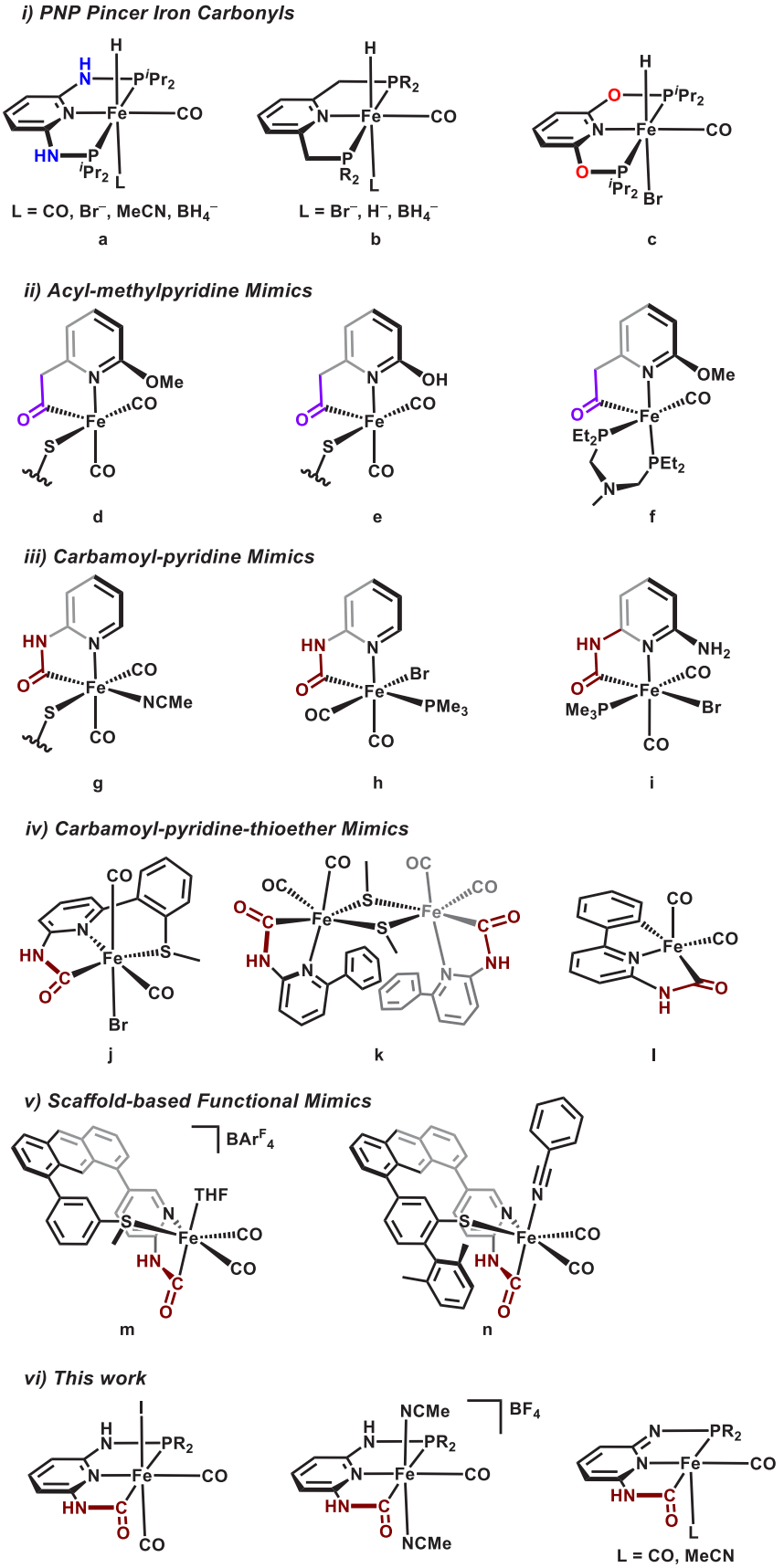

Scheme 3. Synthesis of Monosubstituted Phosphine Ligands (L_{Ph} and L_{iPr}) and Dicarbonyl Iron(II) Complexes (1, 2, 3, and 4)

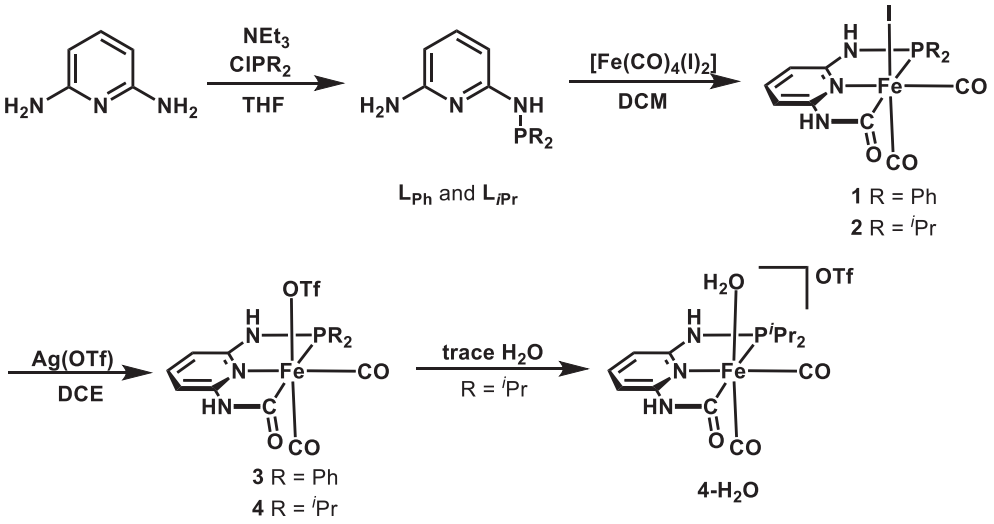

Table 1. Selected Bond Lengths and Bond Angles

complex	3	4-H_2O	7	*cis*-8	*trans*-8	*cis*-9
			Bond Lengths (Å)			
Fe−(C)carbamoyl	1.969(5)	1.962(10)	1.972(7)	1.959(4)	1.955(4)	1.963(2)
Fe−P	2.3037(14)	2.288(3)	2.2729(18)	2.2769(10)	2.2930(11)	2.2976(5)
Fe−N^{Py}	1.947(4)	1.940(8)	1.957(5)	1.937(3)	1.963(3)	1.9456(16)
N(−P)−C^{Py}	1.372(6)	1.377(14)	1.343(9)	1.372(5)	1.366(6)	1.362(3)
N−P	1.690(4)	1.711(9)	1.658(6)	1.701(4)	1.696(4)	1.7012(17)
Fe−C(≡O)$^{in\text{-}plane}$	1.792(5)	1.809(12)	1.778(7)		1.793(4)	
Fe−C(≡O)$^{out\text{-}of\text{-}plane}$	1.751(7)	1.722(13)	1.831(8), 1.793(7)[a]	1.770(5)		1.765(2)
C≡O$^{in\text{-}plane}$	1.149(6)	1.109(14)	1.089(9)		1.139(5)	
C≡O$^{out\text{-}of\text{-}plane}$	1.146(7)	1.150(17)	1.118(8), 1.198(7)[a]	1.143(5)		1.147(3)
Fe−I			2.4984(15), 2.4929(14)[a]			
Fe−NCMe				1.974(4),[b] 1.932(4)	1.916(3), 1.908(4)	1.9717(17), 1.9291(17)
Fe−OH_2		2.001(9)				
Fe−OTf	2.064(5)					
			Bond Angles (deg)			
(O=)C−Fe−P	163.60(16)	165.0(3)	161.3(2)	164.94(14)	164.01(13)	164.29(6)
N^{Py}−Fe−P	81.86(12)	82.4(2)	79.74(17)	82.23(9)	81.81(10)	82.24(5)
MeCN−Fe−NCMe				86.11	175.76	87.15(7)

[a]Substitutional disorder of CO and I. [b]*trans* to CO.

RESULTS AND DISCUSSION

Synthesis, Spectroscopy, and X-ray Structure of Dicarbonyl Complexes. The CNP pincer complexes herein are derived from monosubstituted phosphine ligands (L_{Ph} and L_{iPr}; see Scheme 3), which were synthesized by a nucleophilic substitution reaction of 2,6-diaminopyridine and chlorodiphenylphosphine or chlorodiisopropylphosphine (1 equiv) by modification of a reported procedure.[30−32] The metalation of L_{Ph} and L_{iPr} proceeded at room temperature with $[Fe(CO)_4(I)_2]$ in DCM, which generated the dicarbonyl complexes (**1** and **2**) with a bioinspired carbamoyl unit related to Hmd. Complexes **1** and **2** were characterized by nuclear magnetic resonance (^{1}H NMR, ^{31}P{^{1}H} NMR) and infrared (IR) spectroscopy. The ^{1}H NMR spectrum of **1** exhibits features at 9.64 and 8.74 ppm that correspond to carbamoyl-N*H* and phosphino-N*H*, respectively. For **2**, the resonances of NH protons are shifted upfield (8.70 ppm for carbamoyl-N*H*, 6.93 ppm for phosphino-N*H*), indicating the increased electronic density at the Fe center in **2** resulting from the electron-donating isopropyl substituents. In the ^{31}P{H} NMR spectra, complex **1** displays a singlet at 90.8 ppm, whereas complex **2** gives rise to a singlet at 121.2 ppm. The IR spectrum of **1** shows two carbonyl stretches at 2032 and 1976 cm^{-1}, and for **2** the carbonyl peaks are red-shifted to 2019 and 1967 cm^{-1}, because of the stronger (^{i}Pr)$_2$P donor. The CO stretching frequencies are slightly blue-shifted, relative to the native enzyme data (Hmd: 1996, 1928 cm^{-1}; FeGP cofactor: 2004, 1934 cm^{-1}) and comparable to the anthracene-based model complexes ([(Anth·$C^{NH}NS^{Me}$)Fe(CO)$_2$I]: 2031, 1981 cm^{-1}; [(Anth·C^{NH}NS)Fe(CO)$_2$(PhCN)]: 2016, 1956 cm^{-1}).

To provide structural characterization and provide a more labile coordinate site for reactivity studies, the thermodynamically formed dicarbonyl complexes were derivatized by halide abstraction with silver triflate, forming the triflate-bound complex and AgI precipitate. Treatment of a 1,2-dicholoroethane (DCE) solution of complex **1** or **2** with Ag(OTf) resulting in the formation of either the adduct [($C^{NH}N^{NH}P^{Ph2}$)Fe(CO)$_2$(OTf)] (**3**) or the triflate salt [($C^{NH}N^{NH}P^{iPr2}$)Fe(CO)$_2$(OTf)] (**4**), depending on the R group (R = Ph or ^{i}Pr,

https://dx.doi.org/10.1021/acs.inorgchem.9b03476
Inorg. Chem. XXXX, XXX, XXX−XXX

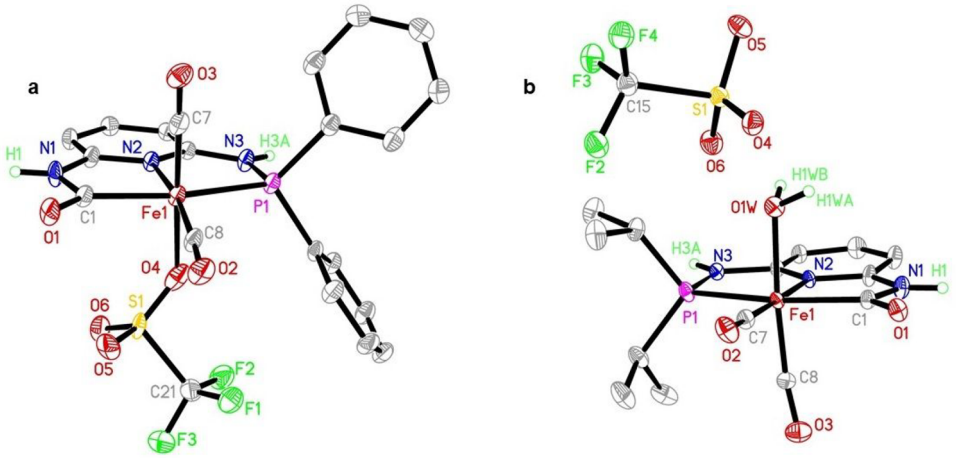

Figure 1. ORTEP diagrams for (a) $[(C^{NH}N^{NH}P^{Ph2})Fe(CO)_2(OTf)]$ (**3**) (30% thermal ellipsoids) and (b) $[(C^{NH}N^{NH}P^{iPr2})Fe(CO)_2(H_2O)](OTf)$ (**4-H$_2$O**) (50% thermal ellipsoids). The H atoms except for the N*H* protons are omitted for clarity.

Scheme 4. Synthesis of Dearomatized Complexes (5, 6)

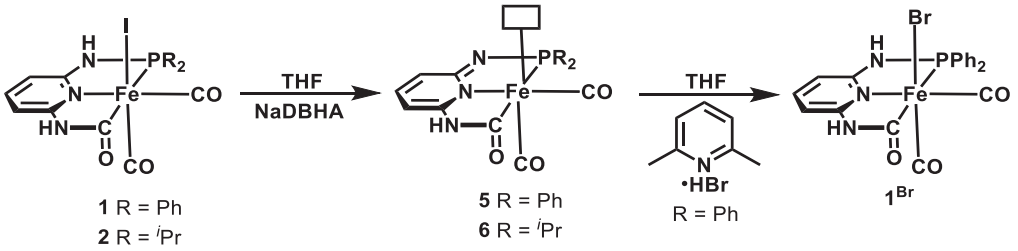

respectively). The IR spectra exhibited the two carbonyl peaks at higher wavenumber (2049, 1993 cm^{-1} for **3**; 2045, 1994 cm^{-1} for **4**) and the ^{31}P resonance of **4** was observed as a singlet at 122.8 ppm. However, the ^{31}P NMR of **3** showed no resonance due to paramagnetic impurity. The crystal structures of the triflate salts were obtained upon recrystallization of the products (vapor diffusion of cyclohexane into the THF solution of complexes). Surprisingly, complex **4** underwent ligand exchange of OTf$^-$ by ambient H_2O during crystallization (the crystallization was set up outside the N_2 box), generating H_2O-bound complex $[(C^{NH}N^{NH}P^{iPr2})Fe(CO)_2(H_2O)](OTf)$ (**4-H$_2$O**). Selected bond parameters and crystal information are tabulated in the Table 1 and Table S1 in the Supporting Information. Complex **3** crystallized as a neutral complex (Figure 1), wherein the Fe center is coordinated with a carbamoyl-C, pyridine-N, and diphenyl-P in the conventional "pincer" equatorial fashion. The CO ligands are arranged in *cis* fashion, and the sixth coordination site is occupied by triflate ligand. The bond distances are unremarkable, except that the Fe−P bond distance (2.3037(14) Å) is longer than regular range of bond length for iron(II) carbonyl phosphine complexes (2.16−2.25 Å).[14,15,17,18,33−36] This is attributed to the *trans* influence of the strongly σ-donating carbamoyl unit.[21] Complex **4** crystallized as a cationic complex, wherein the Fe center is coordinated to the CNP ligand, *cis* CO ligands, and a water molecule—with the charge balance provided by the outer-sphere triflate anion. Presumably, the stronger σ-donating effect of isopropyl-substituted phosphine ligand than diphenylphosphine[37,38] gives rise to (i) the more labile triflate anion due to increased electronic density at the Fe center, and (ii) the Fe−P bond of **4** is slightly shortened (2.288(3) Å), compared with **3** (2.3037(14) Å). Two types of Fe−CO bond are presented in the dicarbonyl complexes; the in-plane CO is further from the Fe center than the axial CO ligand (1.792(5) Å vs 1.751(7) Å in **3**; 1.809(12) Å vs 1.722(13) Å in **4**), which can be ascribed to the stronger *trans* influence of pyridine versus halide/H_2O. This is comparable to the Fe−CO bond length in *cis*-$[Fe(PNP\text{-}^iPr)(CO)_2(Br)]^+$, where the CO in the plane of the ligand backbone has a longer distance to the Fe center, compared with the CO perpendicular to the plane (1.772(1) Å vs 1.758(2) Å).[39] Both complexes display an intermolecular hydrogen bonding motif on the amide proton linkers in the solid state (Figures S37 and S38 in the Supporting Information). The N*H*−P proton interacts with carbamoyl oxygen with bond metrics of O···H = 1.93 Å, O···N = 2.781(7) Å, bond angle = 163° for **3**, and O···H = 1.98 Å, O···N = 2.854(10) Å, bond angle = 174° for **4**. In **4**, the outer sphere triflate anion displays hydrogen bonding with the N*H*−carbamoyl proton with O···H = 2.07 Å, O···N = 2.932(7) Å, bond angle = 168° for **1**, and O···H = 2.10 Å, O···N = 2.913(15) Å, bond angle = 154°.

Activation via Deprotonation/Dearomatization of Dicarbonyl Complexes. Treatment of dicarbonyl complex **1** in THF with 1 equiv of the bulky phenolate, sodium 2,6-di-*tert*-butyl-4-methoxyphenolate (NaDBHA), yielded an orange solution containing the deprotonated/dearomatized product formulated as $[(C^{NH}N^{N=}P^{Ph2})Fe(CO)_2]$ (**5**) (Scheme 4). The ν(CO) peaks were shifted to lower energy at 2006 and 1952 cm^{-1}, indicating deprotonation of the ligand backbone. While the precursor **1** possesses two acidic N*H* protons on the side arms, ^{1}H NMR after deprotonation provides no information on determining the deprotonation site, as the spectrum shows the disappearance of both N*H* resonances. The ^{31}P{^{1}H} NMR spectrum of **5** exhibits a singlet at 90.6 ppm, which is a trivial shift, compared to that of **1** (90.8 ppm). These results may be

https://dx.doi.org/10.1021/acs.inorgchem.9b03476
Inorg. Chem. XXXX, XXX, XXX−XXX

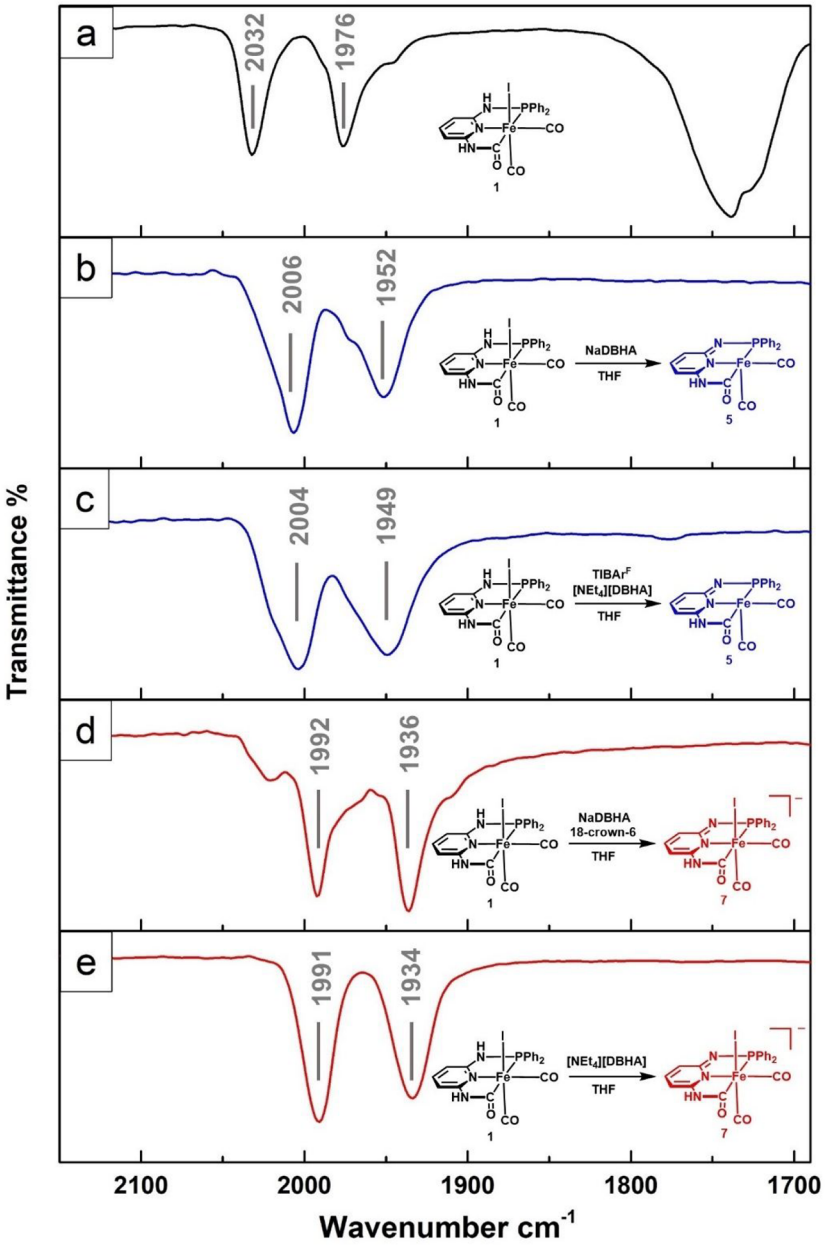

Figure 2. CO region in the IR spectra (drop-cast) of (a) **1** only, (b) reaction of **1** + NaDBHA producing **5**, (c) reaction of **1** + [NEt$_4$][DBHA] + TlBArF producing **5**, (d) reaction of **1** + NaDBHA + 18-crown-6 ether producing **7**, and (e) reaction of **1** + [NEt$_4$][DBHA] producing **7**.

ascribed to a fast proton exchange process the N*H* proton with protic species. Similarly, Kirchner et al. reported a fast proton exchange process between the two N-sites of deprotonated [Fe(PNP-BIPOL)(CH$_3$CN)$_3$]BF$_4$ in MeCN, giving rise to a singlet in ^{31}P{^{1}H} NMR.[40] Since NMR results were ambiguous in determining the exact deprotonation site of **1**, DFT calculations of P−N*H*-deprotonated **5** and carbamoyl N*H*-deprotonated **5′** were performed at PBE0 theory level. The P−N*H*-deprotonated $\mathbf{5}_{DFT}$ is shown to be 12.3 kcal/mol lower than $\mathbf{5'}_{DFT}$ in energy (see Table S2 in the Supporting Information), indicating that the N*H* on the phosphine side arm is deprotonated. The reversibility of the deprotonation was demonstrated by treating **5** with pyridinium bromide in THF, as ^{1}H NMR and IR spectroscopies revealed the regeneration of complex $\mathbf{1}^{Br}$ (Br-bound). For complex **2**, similar deprotonation was observed upon the treatment of NaDBHA and the IR spectrum of the deprotonated complex **6** demonstrated analogously red-shifted CO bands at 2001 and 1942 cm^{-1}, again consistent with deprotonation of the ligand backbone. The ^{31}P{^{1}H} NMR spectrum exhibits a singlet at 116.3 ppm.

To verify the dissociation of iodide from the Fe center in complex **5** (lost as NaI), we substituted NaDBHA with other bases and compared the changes of CO stretches in the solid-state IR spectra recorded via the drop-cast method (see the Supporting Information for details regarding the physical measurements). As shown in Figure 2, treatment of **1** with the corresponding ammonium salt, tetraethylammonium 2,6-di-*tert*-butyl-4-methoxyphenolate ([NEt$_4$][DBHA]) and a halide abstracting reagent, thallium tetrakis(3,5-bis(trifluoromethyl)-phenyl)borate (TlBAr^F), affords an IR spectrum that displays two CO bands at 2004 and 1949 cm^{-1}—similar to those of **5**. This observation means that, in the reaction of NaDBHA and **1**,

https://dx.doi.org/10.1021/acs.inorgchem.9b03476
Inorg. Chem. XXXX, XXX, XXX−XXX

iodide dissociates from the Fe center, forming a pentacoordinate/deprotonated species **5**. Interestingly, the addition of a reagent, [(18-crown-6)Na][DBHA] (Figure 2d) or [NEt_4][DBHA] (Figure 2e) to complex **1** gave rise to two CO peaks red-shifted much further in the solid IR (1992, 1936 cm^{-1} and 1991, 1934 cm^{-1}, respectively). The difference in the CO region can be explained by the formation of an iodide-bound deprotonated species **7**, as evidenced by the crystal structure (vide infra). It is noteworthy that the IR spectra in Figure 2 were obtained by drop casting the sample solution that was taken directly from the reaction. These results indicate that the iodide is so tightly bound to the Fe center that, in solid state, without Tl^+ or Na^+ cation, it ligates the iron, regardless of the deprotonation of the ligand backbone.

While attempts to obtain the X-ray structure of the dearomatized species **5** or **6** were not fruitful, the reaction of **1** with NaDBHA and 1 equiv of 18-crown-6 (Figure 2d) did afford [(18-crown-6)Na][($C^{NH}N^{N=}P^{Ph2}$)Fe$(CO)_2$] (**7**) as orange crystals. The structure of complex **7** exhibits an Fe center coordinated to the CNP ligand, two *cis*-COs and I^- anion, displaying a pseudo-octohedral geometry (Figure 3). Interestingly, the iodide anion shows substitutional disorder, because of its coordination from both sides of the CNP plane (see Figure S39 in the Supporting Information). The occupations of the two isomers are ~50% for each. The 18-crown-6-encapsulated Na^+ cation binds with carbamoyl-O, at a distance of 2.309(5) Å. *Notably, the NH on the phosphine side arm was verifiably deprotonated.* As a result, the N(−P)−C^{Py} and N−P distances are shortened to 1.343(9) Å and 1.658(6) Å, respectively (~1.37 Å and ~1.70 Å for **3** and **4**, respectively). The Fe−P bond length also decreases (2.2729(18) Å), with respect to **3** (2.3037(14) Å) and **4** (2.288(3) Å). The bond angle of P−N−C in **7** is more acute (114°) than those of **3** and **4** (120° and 119°, respectively). In addition, hydrogen bonding is observed between carbamoyl-NH and crown-O (O···H = 2.24 Å, O···N = 3.028(9) Å, bond angle = 153°). Importantly, *no sign of hydrogen bonding is observed on the phosphine side arm*, which is consistent with the deprotonation state of the phosphine-NH linker.

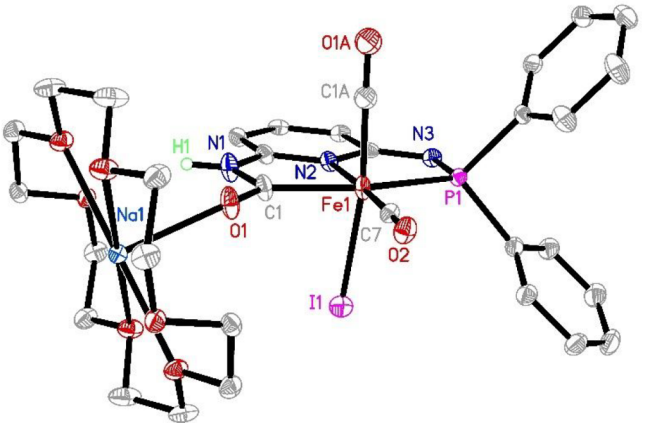

Figure 3. ORTEP diagram (30% thermal ellipsoids) for [Na(18-crown-6)][($C^{NH}N^{N=}P^{Ph2}$)Fe$(CO)_2$I] (**7**). H atoms except for the N*H* proton are omitted for clarity.

Surprisingly, the dissolution of **7** in d^8-THF gives rise to a ^1H NMR spectrum equivalent to that of **5** (Figure 4), and the $^{31}P\{^1H\}$ NMR spectrum of **7** displays a singlet peak at 91.4 ppm, almost the same to the ^{31}P resonance of **5** (90.6 ppm). These

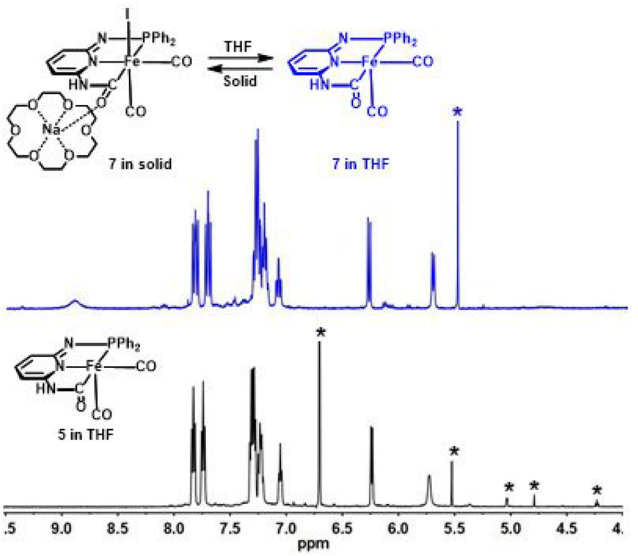

Figure 4. Comparison of ^1H NMR spectra of **7** and **5** in THF-d^8. Peaks corresponding to residual solvent impurity and phenol are labeled with an asterisk (*).

suggest that, in solution, complex **7** loses iodide and converts to the pentacoordinate complex **5**. Similar dehydrohalogenation has been observed or proposed in PNP iron complexes; the deprotonation/dearomatization of the ligand backbone promotes halide dissociation from the Fe center.[14,17] Importantly, such dearomatized and dehalogenated intermediate has been proposed to be the active species to cleave H_2 by the fashion of metal−ligand cooperation.[41] It is promising that the CNP pincer complex could also function as a H_2 activation complex; however, with an anionic carbamoyl unit, the reactivity might be different from the neutral PNP complexes. Since the iodide anion is still dissolved in the solution, upon crystallization, it binds with the Fe center, forming **7**. While the ^1H NMR spectrum of complex **7** matches that of **5**, the ^1H NMR spectrum of **7** exhibits the N*H* resonance at 8.90 ppm, which was not seen in the original spectrum of **5**. This can be attributed to the lack of protic solvent to facilitate proton exchange of N*H*, whereas in **5**, phenol is present, leading to the extinction of the NH peak.

Synthesis of Monocarbonyl Complexes. To study the effect of the number of CO ligands on tuning hydrogen activation reactivity, we synthesized the corresponding monocarbonyl CNP complexes. Direct addition of stoichiometric amounts of the decarbonylating reagent trimethylammonium *N*-oxide (Me_3NO) to **1** resulted in no reaction, and no change in the CO bands was observed in the IR spectroscopy. Meanwhile, treatment of **1** with excessive Me_3NO led only to complete decarbonylation of both CO ligands. The high electron density on the Fe center produces strong backbonding from Fe to CO, which stabilizes CO ligands on Fe. Previously, we reported that decarbonylation can be facilitated by replacing the anionic halide with neutral L-type ligand.[42] Therefore, to attain the monocarbonyl complex **8**, we utilized a two-step synthesis shown in Scheme 5. Starting with **1**, the halide abstracting reagent $AgBF_4$ was added to the acetonitrile solution of **1**, generating the acetonitrile-bound dicarbonyl species. Then, Me_3NO was used to selectively eliminate one CO ligand, affording the monocarbonyl species with two acetonitrile molecules bound in *trans* or *cis* fashion, ***trans*-8** and ***cis*-8**. The IR spectrum of **8** (dropcast) exhibits a single CO band at 1987

https://dx.doi.org/10.1021/acs.inorgchem.9b03476
Inorg. Chem. XXXX, XXX, XXX−XXX

Scheme 5. Synthesis of Monocarbonyl Complexes (*trans*-8 and *cis*-8)

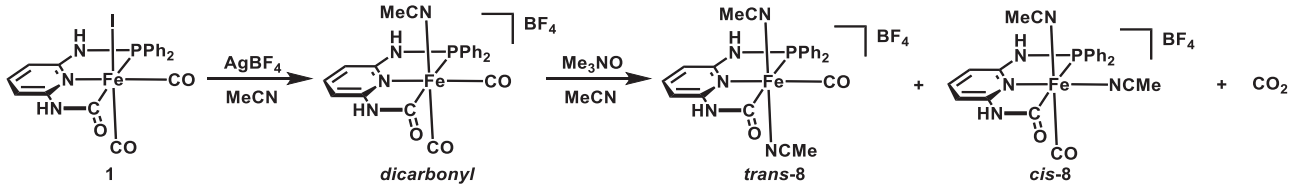

cm^{-1}. In ^{1}H NMR, the *cis* and *trans* isomers can be readily identified at a ratio of ~3:5. The assignments for each feature were based on the ^{1}H−^{31}P HMBC NMR on the isolated product in MeCN-d_3 (see Figure S32 in the Supporting Information). The *cis* isomer exhibits two singlets at 8.85 and 7.88 ppm, which correspond to the carbamoyl-NH and phosphino-NH, respectively. The *trans* isomer displays the specific NH signals at 8.80 and 8.05 ppm. The protons at 5- and 3-positions on pyridine ring give rise to two doublets at 6.47, 6.34 ppm for ***cis*-8** and 6.72, 6.52 ppm for ***trans*-8**. In the aliphatic region, two singlet resonances at 2.31 and 1.74 ppm are attributed to the methyl protons of the coordinated acetonitrile of ***cis*-8**, and the singlet observed at 1.56 ppm corresponds to the methyl protons of ***trans*-8**. These methyl proton resonances persisted for about 1 day and disappeared upon ligand exchange with the deuterated acetonitrile solvent. In ^{31}P{^{1}H} NMR, a singlet is observed at 89.4 ppm for ***cis*-8**, and ***trans*-8** gives rise to a singlet at 100.5 ppm.

The crystal structure of **8** was obtained upon diffusion of diethyl ether to the acetonitrile solution, and, interestingly, ***trans*-8** and ***cis*-8** *co-crystallized* in the crystal lattice. The structure is shown in Figure 5, and the selected bond parameters

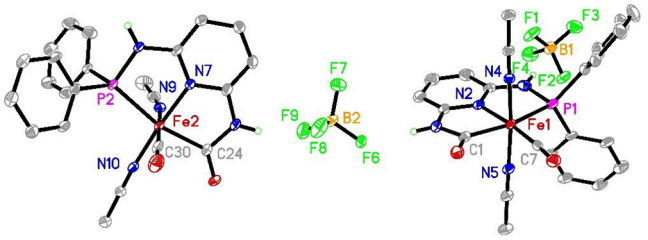

Figure 5. Asymmetric part of the unit cell for **8**: ORTEP diagrams (30% thermal ellipsoids) for *cis*-[($C^{NH}N^{NH}P^{Ph2}$)Fe(CO)$(MeCN)_2$](BF_4) (***cis*-8**) and *trans*-[($C^{NH}N^{NH}P^{Ph2}$)Fe(CO)$(MeCN)_2$](BF_4) (***trans*-8**). Both complexes were found co-crystallized in the same unit cell. H atoms except for the N*H* protons are omitted.

are tabulated in Table 1. Both Fe atoms exhibit pseudo-octahedral geometry and coordinate with the CNP ligand, one CO ligand, and two acetonitrile molecules. The charge of the complex is balanced by BF_4^- anion. The Fe−C(=O) bond distances are shortened (1.959(4) Å for ***cis*-8** and 1.955(4) Å for ***trans*-8**), compared with dicarbonyl complexes. It is noteworthy that, in ***cis*-8**, the orientation of acetonitrile applies the weakest trans-influence on pyridine, leading to the shortest Fe−N^{py} bond length (1.937(3) Å) among all the structures. The Fe−NCMe bond distances are among comparable range of iron(II) acetonitrile bond distance,[40,43−45] except for the longest Fe(2)−N(9) bond (1.974(4) Å).

While room-temperature synthesis of the monocarbonyl complexes afforded ***trans*-8** as the major product, conversion of ***trans*-8** to ***cis*-8** was observed at elevated temperature. The solution of **8** in MeCN-d_3 was heated at 55 °C and NMR spectra were recorded along with the reaction. As shown in Figure 6, the ^{1}H NMR resonances derived from ***trans*-8** gradually decreased, as those of ***cis*-8** increased; the same trend was observed in the ^{31}P NMR spectrum. These results indicate that ***trans*-8** is the kinetic product and ***cis*-8** is the thermodynamic product.

The energy difference between ***cis*-8** and ***trans*-8** was obtained through DFT calculation by geometry optimization at PBE0/opt (see the Supporting Information for details of the basis set) level of theory. The converged structures (see Figures S44 and S45 in the Supporting Information) precisely simulated the structural characteristics of **8**, indicating the accuracy of PBE0 in structural calculation with transition-metal complexes. Importantly, the electronic energy of ***cis*-8** is lower than ***trans*-8** by ~1.5 kcal/mol (see Table S2 in the Supporting Information). This result is consistent with the NMR study of conversion of the *trans* isomer to the *cis* isomer.

The isopropyl analogue complex **9** was synthesized by the similar method, in which we only isolated the ***cis*-9** in 75% yield. A small amount (~8%) of ***trans*-9** complex could be observed from the crude NMR (see Figures S33 and S34 in the Supporting Information). The ^{1}H NMR displays the N*H* protons at 8.75 and 6.86 ppm, which are assignable to carbamoyl NH and phosphine NH, respectively. The signals of isopropyl protons exhibit in an asymmetric pattern, because the *cis* acetonitrile ligands make the two isopropyl groups chemical unequivalent (methine: 2.82, 2.69 ppm; methyl: 1.46−1.27 ppm). The ^{31}P NMR shows a singlet at 110.6 ppm, lower than ***cis*-8**. The CO stretching frequency of ***cis*-9** appears at 1969 cm^{-1}, red-shifted relative to **8**, indicating a higher electron density on the Fe of ***cis*-9**. The crystal structure of ***cis*-9** is shown in Figure 7, and the selected bond parameters are tabulated in Table 1. The Fe atom coordinates with the CNP ligand, one CO ligand, and two *cis*-acetonitrile molecules in a pseudo-octahedral geometry. The Fe−C(=O) bond distance is comparable with **4** (1.963(2) Å for ***cis*-9** and 1.962(10) Å for **4**). Note that, in ***cis*-9**, the Fe−P bond length (2.2976(5) Å) is the longest among all the structures.

H_2 Reactivity. Having proven that the *phospho*ramide NH of CNP complexes can be deprotonated, the possibility of the CNP pincers performing H_2 cleavage was investigated. This would be consistent with numerous literature examples of organometallic iron pincer complexes. Kirchner et al. reported that the dearomatized $P^{NH}N^{NH}P$−Fe pincer complex cleaves H_2, the proton of which protonates the ligand backbone and the hydride binds to the Fe center.[14] Milstein et al., synthesized a series of methylene-derived $P^{CH2}N^{CH2}P$−Fe complexes, which perform hydrogenation of aldehydes, ketones, and trifluoroacetic esters with high efficiency.[17,19,46] The active species of methylene-deprotonated intermediate is also proven spectroscopically and computationally to be critical for hydrogen splitting and hydride transfer. Note that the organometallic pincer complexes are mostly constructed via neutral phosphine tridentate ligands. It is likely that, in our CNP complexes, the increase of the negative charge of the ligand backbone from neutral to −1 would increase

https://dx.doi.org/10.1021/acs.inorgchem.9b03476
Inorg. Chem. XXXX, XXX, XXX−XXX

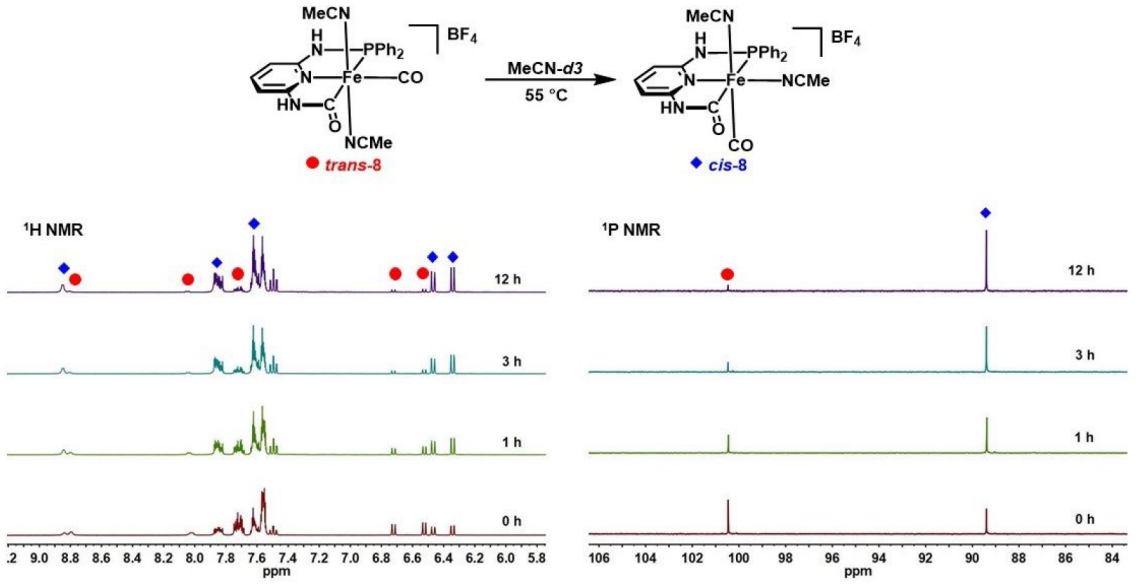

Figure 6. ^{1}H NMR and ^{31}P{^{1}H} NMR spectra showing interconversion of *trans*-[($C^{NH}N^{NH}P^{Ph2}$)Fe(CO)(MeCN)$_2$](BF$_4$) (*trans*-**8**) to *cis*-[($C^{NH}N^{NH}P^{Ph2}$)Fe(CO)(MeCN)$_2$](BF$_4$) (*cis*-**8**) in MeCN-d^3 solution incubated at 55 °C.

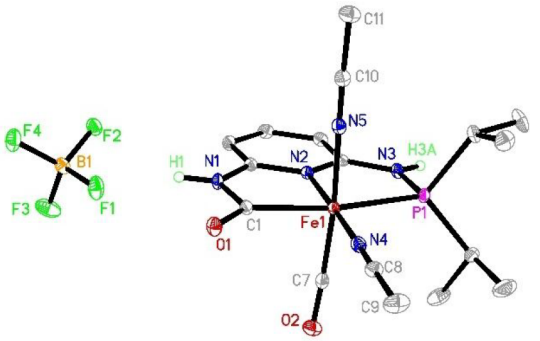

Figure 7. ORTEP diagrams (30% thermal ellipsoids) for *cis*-[($C^{NH}N^{NH}P^{iPr2}$)Fe(CO)(MeCN)$_2$](BF$_4$) (***cis*-9**). H atoms except for the N*H* protons are omitted.

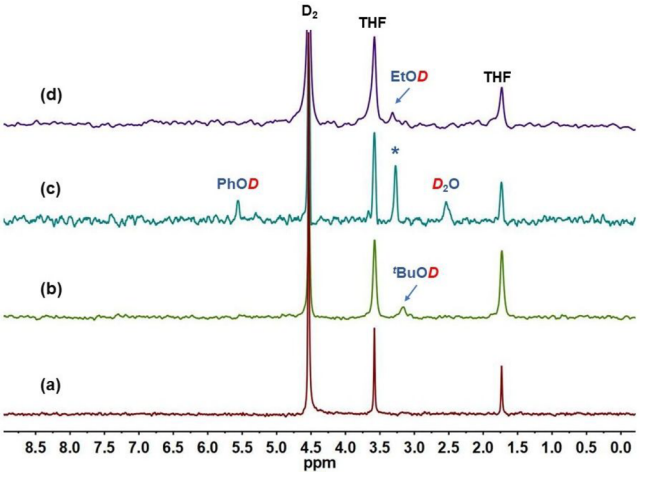

Figure 8. ^{2}H NMR spectra of D_2 activations with dicarbonyl complex **1** or monocarbonyl complex **8**. Reaction conditions: (a) **1** + D_2 (7 atm) + KO^{t}Bu (1 equiv), THF, RT, 1 d; (b) **1** + D_2 (7 atm) + KO^{t}Bu (2 equiv), THF, RT, 1 d; (c) **8**+ D_2 (4 atm) + NaDBHA (1 equiv), THF, RT, 2 d; (d) **8** + D_2 (4 atm) + NaDBHA (1 equiv) + EtOH, THF, RT, 2 d. The identity of the asterisk (*) feature in spectrum (c) remains unknown.

the reactivity in H_2 activation. Moreover, in relation to the bioinspiration for Hmd, we hypothesized that the non-biomimetic monocarbonyl motif would provide a reactivity advantage over the dicarbonyl motif found in the enzyme, because of the higher electron density on the Fe center.

To test these hypotheses, we performed the H_2 activation studies using D_2 and ^{2}H NMR spectroscopy. To a high-pressure NMR tube were charged the THF solution of complexes (**1** or **8**, dicarbonyl and monocarbonyl complexes, respectively), base (bulky phenolate or KO^{t}Bu), and D_2 gas (4−7 atm); after a specified time period, ^{2}H NMR spectra were obtained to identify the formation of deuterated products. As shown in Figure 8a, treatment of dicarbonyl complex **1** with D_2 and 1 equiv of either NaDBHA (weaker phenolate base) or KO^{t}Bu (stronger alkoxide base) did not result in any product peak, as evidenced by the ^{2}H NMR spectrum. However, inclusion of 2 equiv of KO^{t}Bu resulted in a new feature at 3.16 ppm assigned to the *tert*-butanol O*D* resonance (Figure 8b), indicating heterolytic D_2 cleavage. The ^{t}BuO*D* formation suggests that D_2 is cleaved by the exogenous *tert*-butanoxide base. It is evident that the deprotonated ligand backbone does not participate in the reaction, because of the absence of N*D* signal in ^{2}H NMR. In addition, the putative Fe−*D* intermediate was not detected.

By comparison, complex **8** was found to readily activate D_2 gas (4 atm) in the presence of only 1 equiv of the weaker base NaDBHA (Figure 8c). The ^{2}H NMR spectrum exhibited two product peaks at 5.56 and 2.56 ppm, assigned to deuterated 2,6-di-*tert*-butyl-4-methoxyphenol (PhO*D*) and D_2O, respectively, as well as a feature at 3.27 ppm, which was derived from an as-yet-unidentifiable alcohol −O*D* resonance, while the D_2 splitting was not observed in the control experiments without complex (same concentration of NaDBHA + 7 atm D_2 in THF). However, attempts to detect the putative iron deuteride species with NMR were also not fruitful, even at lower temperature (−40 °C). It is likely that the low concentration, as well as the transient nature of the deuteride species, prohibited its detection.

Previously, it has been proposed that ethanol can promote H_2 cleavage catalyzed by a $P^{NH}N^{NH}P$ iron complex by forming a

https://dx.doi.org/10.1021/acs.inorgchem.9b03476
Inorg. Chem. XXXX, XXX, XXX−XXX

proton shuttle between the ligand-backbone pendant base and the iron-bound dihydrogen molecule, thus decreasing the reaction barrier for H_2 splitting.[15,47] To examine this possibility, 20 μL of ethanol (~65 equiv) was added to the reaction containing **8** (Figure 8d). Surprisingly, the reactivity of **8** decreased, as the ^{2}H NMR spectrum only showed a negligible peak attributed to EtO*D* signal and no features assignable to PhO*D* or D_2O was observed. The same result was also obtained when NaDBHA was substituted by KO^{t}Bu. The disappearance of PhO*D* and D_2O peaks indicates that the smaller-sized ethoxide, generated by NaDBHA or KO^{t}Bu, was involved in D_2 cleavage, instead of the bulkier phenolate or *tert*-butoxide, because it was easier for ethoxide to approach the Fe center. Furthermore, the decreased reactivity of **8** is likely due to the coordination of ethanol molecule to the Fe center, leading to a lower amount of the active species cleaving D_2. Overall, the adverse effect of ethanol toward D_2 activation suggests that the ligand−metal cooperation pathway in which D_2 is cleaved by Fe center and the deprotonated NH moiety is not feasible. It is external bases, e.g., *tert*-butoxide, bulky phenolate, or ethoxide, that actually facilitate the reaction.

The aforementioned reactions were also investigated in MeCN as solvent in lieu of THF. The ^{2}H NMR spectra display no resonances for deuterated species, except for those derived from solvent and D_2. This result indicates that D_2 is activated upon binding to the Fe center; with MeCN as a solvent, the vacant site of Fe center is occupied by MeCN, which precludes any reactivity with D_2.

Next, we investigated the D_2/deuteride transfer reactivity of **1** and **8** to assess the possibility of CNP complexes to perform the complete Hmd-relevant process. Complexes **1** or **8** were treated with D_2, base and a deuteride acceptor—such as an imidazolium cation (1,3-bis(2,6-difluorophenyl)-2-(*p*-tolyl)imidazolium, Im^+), or the more strongly deuteride-accepting acridinium cation (9-phenyl-10-methylacridinium, Ac^+).[48] However, neither ^{2}H NMR spectroscopy nor mass spectrometry could detect the corresponding deuteride-transferred product, Im−*D* or Ac−*D*. The lack of deuteride transfer could be attributed to the high Lewis acidity of the Fe center. Bound with only one anionic donor, carbamoyl unit, as well as strong π-accepting CO ligand, the Fe center functions as a deuteride acceptor, rather than a deuteride donor.

DFT Study of H_2 Activation. Based on the above reactivity study, it is evident that the monocarbonyl complex exhibits higher reactivity in H_2 activation than the dicarbonyl complex. To obtain theoretical insight, DFT was used to investigate H_2 binding and activation. Three putative pentacoordinate active species were considered (Scheme 6): the dicarbonyl complex ($\mathbf{A_{diCO}}$), the monocarbonyl complex with MeCN *trans* to the vacant site ($\mathbf{A_{MeCN}}$), and the monocarbonyl complex with CO *trans* to the vacant site ($\mathbf{A_{CO}}$). According to the experimental evidence, the basic amide linker on the ligand backbone does not participate in the reaction (vide infra). We therefore considered

Scheme 6. Dearomatized Pentacoordinate Complexes Considered in the DFT Calculations

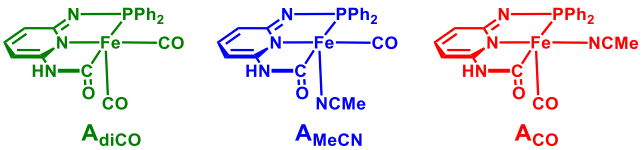

$\mathbf{A_{diCO}}$ $\mathbf{A_{MeCN}}$ $\mathbf{A_{CO}}$

a base-assisted mechanism by calculating the enthalpy change (ΔH) of two subsequent steps involving dearomatized ligand backbone and external bases: (i) H_2 binding to the pentacoordinate dearomatized complexes (**A**), generating H_2 adducts (**B**); and (ii) H_2 cleavage by external bases, forming hydride intermediates (**C**). The ΔH via the reaction trajectory is illustrated in Figure 9 and the enthalpies of base molecules have

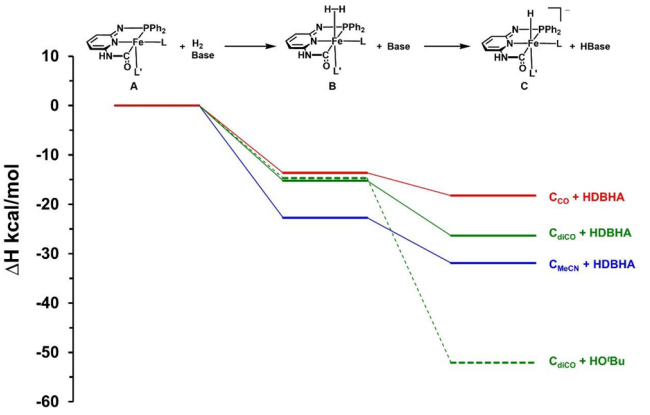

Figure 9. Calculated relative enthalpies in the H_2 binding and cleavage reactions with external bases of $\mathbf{A_{CO}}$ + NaDBHA (red), $\mathbf{A_{diCO}}$ + NaDBHA (solid green), $\mathbf{A_{MeCN}}$ + NaDBHA (blue) and $\mathbf{A_{diCO}}$ + KO^{t}Bu (dashed green) proceeding from the corrected iso-energetic state **A** through **B** and forming **C**.

been taken into account in the total energy calculation, as shown in the equation in Figure 9. In addition, we must point out that the ΔG values of the reactions are dominated by ΔH as the entropy change is negligible ($T\Delta S_{\mathbf{A}\rightarrow\mathbf{B}} = -4.96$ kcal/mol), and, therefore, it is convenient to only consider the enthalpy change in these reactions.

First, the H_2 binding processes are all exothermic. $\mathbf{A_{MeCN}}$ shows the highest affinity for H_2 ($\Delta H_{\mathbf{A}\rightarrow\mathbf{B}} = -22.7$ kcal/mol) and $\mathbf{A_{CO}}$ has the lowest affinity for H_2 ($\Delta H_{\mathbf{A}\rightarrow\mathbf{B}} = -13.6$ kcal/mol) with $\mathbf{A_{diCO}}$ exhibiting a moderate affinity ($\Delta H_{\mathbf{A}\rightarrow\mathbf{B}} = -15.2$ kcal/mol) (Figure 9). While all three Fe complexes exhibit some affinity for H_2, the difference in reactivities does not solely lie on the number of CO ligands—i.e., the electron density at the Fe center. The lowest $\Delta H_{\mathbf{A}\rightarrow\mathbf{B}}$ for **MeCN** and the similar $\Delta H_{\mathbf{A}\rightarrow\mathbf{B}}$ values between **diCO** and **CO** suggest that the ligand *trans* to the H_2 binding site determines the H_2 affinity. According to Kubas principles,[49−51] the Fe−H_2 interaction resembles the classic Dewar−Chatt−Duncanson model, in which the filled $\sigma(H_2)$ donates electron density to the empty $d_{x^2-y^2}$(Fe) orbital, forming a σ-bond, and the filled d_{xy}(Fe) back-donates electron density to $\sigma^*(H_2)$, forming a π-interaction. By examining the MO diagram of **B** (see Figure S57 in the Supporting Information), we identified the σ bonding orbital of Fe−H_2 for the complexes in low energy orbitals (HOMO−40 for $\mathbf{B_{CO}}$; HOMO−27 for $\mathbf{B_{diCO}}$; MOHO−45 for $\mathbf{B_{MeCN}}$) and the π-interaction emerging from back-donation are closer to the frontier orbitals: HOMO−5 for $\mathbf{B_{CO}}$; HOMO−8 for $\mathbf{B_{diCO}}$; MOHO−4 for $\mathbf{B_{MeCN}}$. The weak π-accepting ligand MeCN *trans* to the vacant site is less competitive (versus *trans* CO) with H_2 for back-donation from d_{xz}(Fe)—which is an orbital that the two *trans* ligands (H_2 and MeCN/CO) must share.[52] Therefore, the *trans* MeCN case provides the strongest Fe−H_2 bonding interaction in the set.

Notably, the identity of the external base does not have an apparent influence on ΔH of the H_2 binding process. For the dicarbonyl complex $\mathbf{A_{diCO}}$, changing the base from NaDBHA

https://dx.doi.org/10.1021/acs.inorgchem.9b03476
Inorg. Chem. XXXX, XXX, XXX−XXX

Table 2. Reaction Optimization for Transfer Hydrogenation of ^{i}PrOH to Benzylaldehyde[a]

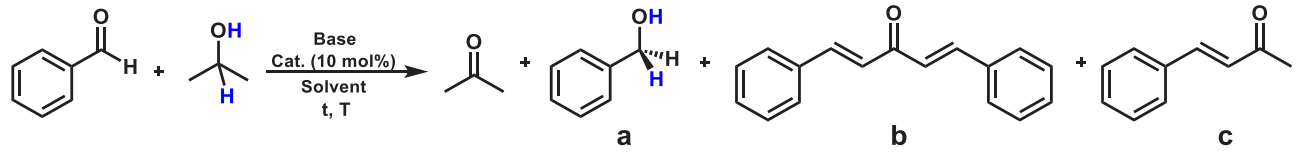

entry	catalyst (10 mol %)	time, t (h)	base	base equiv	temperature, T (°C)	solvent	conversion (%)	Yield[c] (%) a	b	c	turnover number, TON[d]
1	**8**	20	NaDBHA	1	60	^{i}PrOH	0	0	0	0	
2	**8**	20	NaDBHA	2	60	^{i}PrOH	3	1	0	0	
3	**8**	20	NaDBHA	3	60	^{i}PrOH	87	22	53	6	2
4	**8**	20	NaDBHA	3	40	^{i}PrOH	33	21	3	7	2
5	**8**	20	NaDBHA	3	RT	^{i}PrOH	4	2	0	2	
6	**8**	20	DBU	3	40	^{i}PrOH	0	0	0	0	
7	**8**	20	KO^{t}Bu	3	40	^{i}PrOH	38	17	11	9	2
8	**8**	20	KOH	3	40	^{i}PrOH	34	18	7	8	2
9	**8**	20	KOH	3	60	^{i}PrOH	53	35	7	11	3
10	**8**	20	KOH	3	80	^{i}PrOH	84	31	51	2	3
11	**8**	20	NaDBHA	3	40	^{i}PrOH+H_2O[b]	3	3	0	0	
12	**8**	20	KO^{t}Bu	3	40	^{i}PrOH+H_2O	26	8	11	6	
13	**8**	20	KOH	3	40	^{i}PrOH+H_2O	2	2	0	0	
14	**8**	1	KOH	3	80	^{i}PrOH	83	29	47	7	3
15	**1**	20	KOH	3	80	^{i}PrOH	40	18	22	1	2
16	–	20	KOH	3	80	^{i}PrOH	37	13	23	1	1
17	**9**	20	KOH	3	80	^{i}PrOH	58	21	32	5	2

[a]General reaction conditions: 0.0157 mmol of base, 0.0523 mmol of benzylaldehyde, 10 mol % of catalyst, 1 mL of solvent. [b]0.9 mL ^{i}PrOH + 0.1 mL H_2O. [c]Yields calculated from the integration of GC-MS data. [d]TON = (mmol of benzyl alcohol)/(mmol of catalyst).

(solid green line in Figure 9) to KO^{t}Bu (dashed green line) slightly increases the enthalpy of the system (from −15.2 kcal/mol to −14.7 kcal/mol). This is reasonable in that the base is not directly participating in this step.

Next, we considered the energy change of the H_2 cleavage step via base-assisted mechanism, in which H_2 on **B** is heterolytically cleaved, producing hydride intermediate **C** and conjugate acid. When NaDBHA is chosen as a base (Figure 9, solid lines), all three complexes give rise to exothermic results in which $\mathbf{C}_{\mathbf{MeCN}}$ shows the lowest energy (−31.9 kcal/mol), $\mathbf{C}_{\mathbf{diCO}}$ in the middle (−26.4 kcal/mol), and $\mathbf{C}_{\mathbf{CO}}$ is the highest in energy (−18.2 kcal/mol). Although the $\Delta H_{\mathrm{B}\rightarrow\mathrm{C}}$ values are comparable for all three complexes, the total $\Delta H_{\mathrm{A}\rightarrow\mathrm{C}}$ for all three reactions shows clear trend in that the monocarbonyl complex $\mathbf{A}_{\mathbf{MeCN}}$ is the most reactive species in H_2 activation and, significantly, $\mathbf{A}_{\mathbf{CO}}$ is the least active species among them, indicating that $\mathbf{A}_{\mathbf{CO}}$ is not responsible for H_2 activation. This is consistent with the experimental evidence that monocarbonyl complex **8** is more easily activated (1 equiv of NaDBHA is sufficient for H_2 heterolysis). Interestingly, substitution of NaDBHA for KO^{t}Bu led to a drastic decrease in enthalpy for **diCO** (−52.1 kcal/mol), making the H_2 cleavage with $\mathbf{A}_{\mathbf{diCO}}$ complex more feasible. This is in agreement with the experimental results showing that dicarbonyl complex **1** was able to activate H_2 in the presence of 2 equiv KO^{t}Bu. These results demonstrate that the propensity of H_2 cleavage is highly dependent on the basicity of the external base.

The calculated energy profile demonstrates the additive effects of the *trans* influence in the primary coordination sphere and the basicity of external bases in H_2 activation. Both theoretically and experimentally, we have showed that the monocarbonyl complex $\mathbf{A}_{\mathbf{MeCN}}$ is the most reactive among the three. Importantly, although the number of CO ligands does affect the electron density of the Fe center, it seems that the identity of the *trans* ligand to the H_2 binding site is more pivotal in our pincer system. The *trans* MeCN ligand features weak σ-donating and weak π-accepting ability, which promotes the bonding of H_2 to Fe center. This strategy has also been utilized by [Fe]-hydrogenase, as the acyl moiety is a strong σ-donor and weak π-acceptor and unquestionably enables the enzyme to exhibit a stronger affinity for H_2. Therefore, we believe this is a crucial way to modulate *trans* influence to tune the activity of catalysts for H_2 activation.

Transfer Hydrogenation. The affinity of CNP complexes to bind alcohols (vide supra) prompted us to test their function as transfer hydrogenation (TH) catalysts to demonstrate the functional reactivity of the CNP system. The selected reaction was transfer hydrogenation of benzylaldehyde using ^{i}PrOH as a hydrogen source. A complete screening of the base, temperature, solvent, and catalysts was performed (see Table 2). Starting with the monocarbonyl complex **8** and NaDBHA as a base at 60 °C, increasing to the amount of NaDBHA to 3 equiv led to higher reactivity with 87% of conversion of benzylaldehyde (see Table 2, entry 3). However, GC-MS results revealed the major product to be the dienone **b** (53%) with the minor product as enone **c** (6%). The desired hydrogen-transferred product benzyl alcohol **a** formed with yield of 22%. The side products **b** and **c** were produced from the Claisen−Schmidt condensation in which acetone reacted with benzylaldehyde under basic conditions.[53] Decreasing the temperature provided smaller amounts of side products (see Table 2, entries 4 and 5), but the yield of benzyl alcohol also decreased. Screening of different bases revealed that the neutral nitrogen-based base, 1,8-diazabicyclo[5.4.0]undec-7-ene (DBU), is not suitable to promote the reaction, most likely

https://dx.doi.org/10.1021/acs.inorgchem.9b03476
Inorg. Chem. XXXX, XXX, XXX−XXX

because of its weaker basicity (Table 2, entry 6). Instead, using the strong inorganic base KOH (Table 2, entry 8) afforded a higher yield of benzyl alcohol and lower formation of side products, compared with other organic bases (NaDBHA, DBU, and KO^{t}Bu). The optimal temperature with KOH was determined to be 60 °C, with the highest yield of **a** at 35% (Table 2, entries 9 and 10). Water has also been reported to benefit the TH reaction with PNP complexes, because of its formation of a proton bridge, which facilitates the proton transfer between the pendant base and the substrate.[47] However, the addition of ∼10% water (V_{H_2O}:$V_{^iPrOH}$ = 1:9) to the reaction mixture suppressed the reaction, regardless of the base identity (Table 2, entries 11−13). Shortening the reaction time from 20 h to 1 h (Table 2, entry 14) resulted in only a slightly lower yield of **a** (29%), indicating that benzylaldehyde was hydrogenated within the first hour of reaction. Lastly, the effects of changing complexes on TH were investigated. Exchanging the monocarbonyl complex **8** for the *dicarbonyl* complex **1** led to decrease of the yield of **a** to 18% (Table 2, entry 15), indicating lower catalytic activity of the dicarbonyl system. It is noteworthy that, in the absence of Fe complex, the TH reaction still occurred, with benzyl alcohol formed at 13% yield (Table 2, entry 16). Indeed, it has been reported that quantitative reduction of acetophenone to phenylethanol was observed in a concentrated NaOH solution.[54] Surprisingly, substituting the isopropyl monocarbonyl analogue (with −P^{i}Pr$_2$) complex **9** for **8** (with −PPh$_2$) again provided a lower yield (21%; see Table 2, entry 17). This is comparable to the reaction with **1**, indicating that the isopropyl substitution does not promote the TH reactivity in this series of CNP complexes.

Although some catalytic activity was observed with our CNP complexes, the overall performance of the catalysts does not compare favorably with other well-established catalysts.[55] Such low TH activity could be due to the low hydricity of the hydride species (thermodynamic hydride donating ability),[56] considering that the active species in TH is usually a metal-hydride intermediate.[55] For example, Hu reported the [Fe(H)(Br)-(^{i}Pr$_2$PONOP ^{i}Pr$_2$)] catalyzes the TH reaction to aldehydes using formate as the hydride source, in which the dihydride species [Fe(H)$_2$(^{i}Pr$_2$PONOP ^{i}Pr$_2$)] was proposed to be the active species.[20] Although we have not yet observed the hydride intermediate in the present set of CNP complexes, it is reasonable to hypothesize that the catalytic cycle involves the formation of hydride species. In the previous section, we have established the energy profile of H_2 cleavage with the CNP complexes. The DFT calculations suggest high stability of the hydride species (**C**), which likely results in weak hydricity and, thus, TH activity.

CONCLUSION

The main conclusions of this work can be summarized as follows:

(1) Bioinspired iron(II) carbonyl pincers are synthetically accessible via metalation of the apo-ligand with a ferrous carbonyl salt, which forms the Fe−C(carbamoyl) bond in situ.

(2) Base addition results in deprotonation of the phosphoramide unit (analogous to the Kirchner system), rather than the carbamoyl unit.

(3) Incubation of the pentacoordinate dearomatized/deprotonated complexes in D_2 gas leads to the appearance of the PhO*D* or ^{t}BuO*D* signals in ^{2}H NMR spectroscopy, indicating the heterolytic cleavage of D_2 with the CNP complexes. Conditions for reactions (1 equiv of PhONa for **8** and 2 equiv of KO^{t}Bu for **1**) show that monocarbonyl complex **8** exhibits higher reactivity for H_2 activation than dicarbonyl complex **1**.

(4) DFT calculations show that the efficiency of H_2 reactivity follows the trend of **CO** < **diCO** < **MeCN**. This reactivity difference is largely derived from the step of H_2 binding, in which electron density at the Fe center (minor effect) and influence of ligand *trans* to the H_2 binding site (major effect) jointly modulate the affinity of H_2 of the pentacoordinate species (**A**). Subsequently, the cooperation of the Fe center and external bases leads to H_2 cleavage. The efficiency should be related to the pK_a of the base and the extent of H−H bond weakening, which are consistent with the experimental results.

(5) The catalytic activity of the monocarbonyl CNP complex **8** toward transfer hydrogenation of benzylaldehyde is observed, whereas the dicarbonyl complex **1** and −P^{i}Pr$_2$-substituted complex **9** exhibit lower to no reactivity. This could be ascribed to the latter species' more-stable hydride species, leading to low hydricity and hydride transfer.

(6) These results highlight three key items regarding the [Fe]-hydrogenase enzyme:

(i) The counterintuitive use of the less H_2-reactive dicarbonyl motif may restrain the reactivity of [Fe]-hydrogenase, thus providing more selectivity for hydride transfer to the imidazolium unit of the H_4MPT^+.

(ii) The methylene-acyl carbanion present in the active site occurs trans to the site of H_2 activation; this strong σ donor and weak π acceptor likely drives significant H−H elongation in the putative Kubas intermediate.

(iii) The pyridone/pyridonate-O atom directly adjacent to the H_2 binding site in the enzyme likely provides both the optimum *basicity and orientation* that promotes H_2 heterolysis ($\Delta E_a \approx 1$ kcal/mol, as estimated via the QM/MM method).[13]

(7) Future bioinspired catalysts (with or without phosphine) should aspire to achieve such a second-coordination sphere feature. In addition, new catalysts and complexes with strong σ-donating and weak π-accepting ligand *trans* to the hydride (e.g., H^-, phosphine, and cyclopentadiene) would increase reactivities toward both H_2 splitting and hydride transfer.

ASSOCIATED CONTENT

Supporting Information

The Supporting Information is available free of charge at https://pubs.acs.org/doi/10.1021/acs.inorgchem.9b03476.

Details of synthetic procedures, NMR spectra, IR spectra, X-ray crystallography, and DFT calculations (PDF)

Accession Codes

CCDC 1907564−1907568 contain the supplementary crystallographic data for this paper. These data can be obtained free of charge via www.ccdc.cam.ac.uk/data_request/cif, or by emailing data_request@ccdc.cam.ac.uk, or by contacting The Cambridge Crystallographic Data Centre, 12 Union Road, Cambridge CB2 1EZ, UK; fax: +44 1223 336033.

AUTHOR INFORMATION

Corresponding Author

Michael J. Rose − *Department of Chemistry, The University of Texas at Austin, Austin, Texas 78712, United States;*

https://dx.doi.org/10.1021/acs.inorgchem.9b03476
Inorg. Chem. XXXX, XXX, XXX−XXX

orcid.org/0000-0002-6960-6639; Email: mrose@cm.utexas.edu

Authors

Zhu-Lin Xie − *Department of Chemistry, The University of Texas at Austin, Austin, Texas 78712, United States;* orcid.org/0000-0002-1969-2831

Wenrui Chai − *Department of Chemistry, The University of Texas at Austin, Austin, Texas 78712, United States;* orcid.org/0000-0002-5801-0135

Spencer A. Kerns − *Department of Chemistry, The University of Texas at Austin, Austin, Texas 78712, United States;* orcid.org/0000-0001-6936-8098

Graeme A. Henkelman − *Department of Chemistry, The University of Texas at Austin, Austin, Texas 78712, United States;* orcid.org/0000-0002-0336-7153

Complete contact information is available at: https://pubs.acs.org/10.1021/acs.inorgchem.9b03476

Notes

The authors declare no competing financial interest.

■ ACKNOWLEDGMENTS

Z.X., S.A.K., and M.J.R. acknowledge funding from the National Science Foundation (NSF) (No. CHE-1808311) and the Welch Foundation (No. F-1822), and are grateful to Dr. Vince Lynch for assistance in solving X-ray structures. W.C. and G.H. acknowledge funding from the Welch Foundation (No. F-1841) and computational resources from the Texas Advanced Computing Center.

■ REFERENCES

(1) Santhanam, K. S. V.; Press, R. J.; Miri, M. J.; Bailey, A. V.; Takacs, G. A. *Introduction to Hydrogen Technology*, 2nd Edition; Wiley: Hoboken, NJ, 2017.

(2) Momirlan, M.; Veziroglu, T. Current Status of Hydrogen Energy. *Renewable Sustainable Energy Rev.* **2002**, *6* (1−2), 141−179.

(3) Zhang, F.; Zhao, P.; Niu, M.; Maddy, J. The Survey of Key Technologies in Hydrogen Energy Storage. *Int. J. Hydrogen Energy* **2016**, *41* (33), 14535−14552.

(4) Møller, K. T.; Jensen, T. R.; Akiba, E.; Li, H. Hydrogen - A Sustainable Energy Carrier. *Prog. Nat. Sci.* **2017**, *27* (1), 34−40.

(5) *Hydrogen Production Technical Team Roadmap*. Technical Report; U.S. Department of Energy Office of Scientific and Technical Information, 2017 (DOI: 10.2172/1220219).

(6) Holladay, J. D.; Hu, J.; King, D. L.; Wang, Y. An Overview of Hydrogen Production Technologies. *Catal. Today* **2009**, *139* (4), 244−260.

(7) Lubitz, W.; Ogata, H.; Rüdiger, O.; Reijerse, E. Hydrogenases. *Chem. Rev.* **2014**, *114* (8), 4081−4148.

(8) Schilter, D.; Camara, J. M.; Huynh, M. T.; Hammes-Schiffer, S.; Rauchfuss, T. B. Hydrogenase Enzymes and Their Synthetic Models: The Role of Metal Hydrides. *Chem. Rev.* **2016**, *116* (15), 8693−8749.

(9) Evans, D. J.; Pickett, C. J. Chemistry and the Hydrogenases. *Chem. Soc. Rev.* **2003**, *32* (5), 268−275.

(10) Shima, S.; Pilak, O.; Vogt, S.; Schick, M.; Stagni, M. S.; Meyer-Klaucke, W.; Warkentin, E.; Thauer, R. K.; Ermler, U. The Crystal Structure of [Fe]-Hydrogenase Reveals the Geometry of the Active Site. *Science* **2008**, *321* (5888), 572−575.

(11) Hiromoto, T.; Ataka, K.; Pilak, O.; Vogt, S.; Stagni, M. S.; Meyer-Klaucke, W.; Warkentin, E.; Thauer, R. K.; Shima, S.; Ermler, U. The Crystal Structure of C176A Mutated [Fe]-Hydrogenase Suggests an Acyl-Iron Ligation in the Active Site Iron Complex. *FEBS Lett.* **2009**, *583* (3), 585−590.

(12) Yang, X.; Hall, M. B. Monoiron Hydrogenase Catalysis: Hydrogen Activation with the Formation of a Dihydrogen, Fe-Hδ−···Hδ+-O, Bond and Methenyl-H4MPT+ Triggered Hydride Transfer. *J. Am. Chem. Soc.* **2009**, *131* (31), 10901−10908.

(13) Finkelmann, A. R.; Senn, H. M.; Reiher, M. Hydrogen-Activation Mechanism of [Fe] Hydrogenase Revealed by Multi-Scale Modeling. *Chem. Sci.* **2014**, *5* (11), 4474−4482.

(14) Bichler, B.; Holzhacker, C.; Stöger, B.; Puchberger, M.; Veiros, L. F.; Kirchner, K. Heterolytic Cleavage of Dihydrogen by an Iron(II) PNP Pincer Complex via Metal-Ligand Cooperation. *Organometallics* **2013**, *32* (15), 4114−4121.

(15) Gorgas, N.; Stöger, B.; Veiros, L. F.; Pittenauer, E.; Allmaier, G.; Kirchner, K. Efficient Hydrogenation of Ketones and Aldehydes Catalyzed by Well-Defined Iron(II) PNP Pincer Complexes: Evidence for an Insertion Mechanism. *Organometallics* **2014**, *33* (23), 6905−6914.

(16) Langer, R.; Diskin-Posner, Y.; Leitus, G.; Shimon, L. J. W.; Ben-David, Y.; Milstein, D. Low-Pressure Hydrogenation of Carbon Dioxide Catalyzed by an Iron Pincer Complex Exhibiting Noble Metal Activity. *Angew. Chem., Int. Ed.* **2011**, *50* (42), 9948−9952.

(17) Langer, R.; Leitus, G.; Ben-David, Y.; Milstein, D. Efficient Hydrogenation of Ketones Catalyzed by an Iron Pincer Complex. *Angew. Chem., Int. Ed.* **2011**, *50* (9), 2120−2124.

(18) Langer, R.; Iron, M. A.; Konstantinovski, L.; Diskin-Posner, Y.; Leitus, G.; Ben-David, Y.; Milstein, D. Iron Borohydride Pincer Complexes for the Efficient Hydrogenation of Ketones under Mild, Base-Free Conditions: Synthesis and Mechanistic Insight. *Chem. - Eur. J.* **2012**, *18* (23), 7196−7209.

(19) Zell, T.; Ben-David, Y.; Milstein, D. Unprecedented Iron-Catalyzed Ester Hydrogenation. Mild, Selective, and Efficient Hydrogenation of Trifluoroacetic Esters to Alcohols Catalyzed by an Iron Pincer Complex. *Angew. Chem., Int. Ed.* **2014**, *53* (18), 4685−4689.

(20) Mazza, S.; Scopelliti, R.; Hu, X. Chemoselective Hydrogenation and Transfer Hydrogenation of Aldehydes Catalyzed by Iron(II) PONOP Pincer Complexes. *Organometallics* **2015**, *34* (8), 1538−1545.

(21) Chen, D.; Scopelliti, R.; Hu, X. A Five-Coordinate Iron Center in the Active Site of [Fe]-Hydrogenase: Hints from a Model Study. *Angew. Chem., Int. Ed.* **2011**, *50* (25), 5671−5673.

(22) Hu, B.; Chen, D.; Hu, X. Synthesis and Reactivity of Mononuclear Iron Models of [Fe]-Hydrogenase That Contain an Acylmethylpyridinol Ligand. *Chem. - Eur. J.* **2014**, *20* (6), 1677−1682.

(23) Xu, T.; Yin, C.-J. M.; Wodrich, M. D.; Mazza, S.; Schultz, K. M.; Scopelliti, R.; Hu, X. A Functional Model of [Fe]-Hydrogenase. *J. Am. Chem. Soc.* **2016**, *138* (10), 3270−3273.

(24) Turrell, P. J.; Hill, A. D.; Ibrahim, S. K.; Wright, J. A.; Pickett, C. J. Ferracyclic Carbamoyl Complexes Related to the Active Site of [Fe]-Hydrogenase. *Dalton Trans.* **2013**, *42* (22), 8140−8146.

(25) Turrell, P. J.; Wright, J. A.; Peck, J. N. T.; Oganesyan, V. S.; Pickett, C. J. The Third Hydrogenase: A Ferracyclic Carbamoyl with Close Structural Analogy to the Active Site of Hmd. *Angew. Chem., Int. Ed.* **2010**, *49* (41), 7508−7511.

(26) Shima, S.; Chen, D.; Xu, T.; Wodrich, M. D.; Fujishiro, T.; Schultz, K. M.; Kahnt, J.; Ataka, K.; Hu, X. Reconstitution of [Fe]-Hydrogenase Using Model Complexes. *Nat. Chem.* **2015**, *7* (12), 995−1002.

(27) Durgaprasad, G.; Xie, Z.-L.; Rose, M. J. Iron Hydride Detection and Intramolecular Hydride Transfer in a Synthetic Model of Mono-Iron Hydrogenase with a CNS Chelate. *Inorg. Chem.* **2016**, *55* (2), 386−389.

(28) Seo, J.; Manes, T. A.; Rose, M. J. Structural and Functional Synthetic Model of Mono-Iron Hydrogenase Featuring an Anthracene Scaffold. *Nat. Chem.* **2017**, *9* (6), 552−557.

(29) Kerns, S. A.; Magtaan, A.-C.; Vong, P. R.; Rose, M. J. Functional Hydride Transfer by a Thiolate-Containing Model of Mono-Iron Hydrogenase Featuring an Anthracene Scaffold. *Angew. Chem., Int. Ed.* **2018**, *57* (11), 2855−2858.

(30) Schroeder-Holzhacker, C.; Stoeger, B.; Pittenauer, E.; Allmaier, G. G.; Veiros, L. F.; Kirchner, K.; et al. High-Spin Iron(II) Complexes with Mono-Phosphorylated 2,6-Diaminopyridine Ligands. *Monatsh. Chem.* **2016**, *147* (9), 1539−1545.

(31) Holzhacker, C.; Stoeger, B.; Carvalho, M. D.; Ferreira, L. P.; Pittenauer, E.; Allmaier, G.; Veiros, L. F.; Realista, S.; Gil, A.; Calhorda, M. J.; et al. Synthesis and Reactivity of TADDOL-Based Chiral Fe(II) PNP Pincer Complexes-Solution Equilibria between K2P, N- and K3P,N,P-Bound PNP Pincer Ligands. *Dalton Trans.* **2015**, *44* (29), 13071−13086.
(32) Lackner-Warton, W.; Tanaka, S.; Standfest-Hauser, C. M.; Öztopcu, Ö.; Hsieh, J.-C.; Mereiter, K.; Kirchner, K. Synthesis and Characterization of Ruthenium P-Cymene Complexes Bearing Bidentate P-N and E-N Ligands (E = S, Se) Based on 2-Aminopyridine. *Polyhedron* **2010**, *29* (16), 3097−3102.
(33) Gorgas, N.; Stöger, B.; Veiros, L. F.; Kirchner, K. Highly Efficient and Selective Hydrogenation of Aldehydes: A Well-Defined Fe(II) Catalyst Exhibits Noble-Metal Activity. *ACS Catal.* **2016**, *6* (4), 2664−2672.
(34) Mastalir, M.; Glatz, M.; Gorgas, N.; Stöger, B.; Pittenauer, E.; Allmaier, G.; Veiros, L. F.; Kirchner, K. Divergent Coupling of Alcohols and Amines Catalyzed by Isoelectronic Hydride Mn ^{I} and Fe ^{II} PNP Pincer Complexes. *Chem. - Eur. J.* **2016**, *22* (35), 12316−12320.
(35) Bertini, F.; Gorgas, N.; Stöger, B.; Peruzzini, M.; Veiros, L. F.; Kirchner, K.; Gonsalvi, L. Efficient and Mild Carbon Dioxide Hydrogenation to Formate Catalyzed by Fe(II) Hydrido Carbonyl Complexes Bearing 2,6-(Diaminopyridyl)Diphosphine Pincer Ligands. *ACS Catal.* **2016**, *6* (5), 2889−2893.
(36) Huber, R.; Passera, A.; Mezzetti, A. Iron(II)-Catalyzed Hydrogenation of Acetophenone with a Chiral, Pyridine-Based PNP Pincer Ligand: Support for an Outer-Sphere Mechanism. *Organometallics* **2018**, *37* (3), 396−405.
(37) Tolman, C. A. Steric Effects of Phosphorus Ligands in Organometallic Chemistry and Homogeneous Catalysis. *Chem. Rev.* **1977**, *77* (3), 313−348.
(38) Crabtree, R. H. Carbonyls, Phosphine Complexes, and Ligand Substitution Reactions. In *The Organometallic Chemistry of the Transition Metals*; John Wiley & Sons, Inc.: Hoboken, NJ, 2005; pp 87−124 (DOI: 10.1002/0471718769.ch4).
(39) Gorgas, N.; Alves, L. G.; Stöger, B.; Martins, A. M.; Veiros, L. F.; Kirchner, K. Stable, Yet Highly Reactive Nonclassical Iron(II) Polyhydride Pincer Complexes: Z-Selective Dimerization and Hydroboration of Terminal Alkynes. *J. Am. Chem. Soc.* **2017**, *139* (24), 8130−8133.
(40) Benito-Garagorri, D.; Becker, E.; Wiedermann, J.; Lackner, W.; Pollak, M.; Mereiter, K.; Kisala, J.; Kirchner, K. Achiral and Chiral Transition Metal Complexes with Modularly Designed Tridentate PNP Pincer-Type Ligands Based on N-Heterocyclic Diamines. *Organometallics* **2006**, *25* (8), 1900−1913.
(41) Hale, L. V. A.; Szymczak, N. K. Hydrogen Transfer Catalysis beyond the Primary Coordination Sphere. *ACS Catal.* **2018**, *8* (7), 6446−6461.
(42) Xie, Z.-L.; Durgaprasad, G.; Ali, A. K.; Rose, M. J. Substitution Reactions of Iron(II) Carbamoyl-Thioether Complexes Related to Mono-Iron Hydrogenase. *Dalton Trans.* **2017**, *46* (33), 10814−10829.
(43) Nakahara, Y.; Toda, T.; Kuwata, S. Iron and Ruthenium Complexes Having a Pincer-Type Ligand with Two Protic Amidepyrazole Arms: Structures and Catalytic Application. *Polyhedron* **2018**, *143*, 105−110.
(44) Aloisi, A.; Berthet, J.-C.; Genre, C.; Thuéry, P.; Cantat, T. Complexes of the Tripodal Phosphine Ligands $PhSi(XPPh_2)_3$ (X = CH_2, O): Synthesis, Structure and Catalytic Activity in the Hydroboration of CO_2. *Dalton Trans.* **2016**, *45* (37), 14774−14788.
(45) Sui-Seng, C.; Freutel, F.; Lough, A. J.; Morris, R. H. Highly Efficient Catalyst Systems Using Iron Complexes with a Tetradentate PNNP Ligand for the Asymmetric Hydrogenation of Polar Bonds. *Angew. Chem., Int. Ed.* **2008**, *47* (5), 940−943.
(46) Zell, T.; Ben-David, Y.; Milstein, D. Highly Efficient, General Hydrogenation of Aldehydes Catalyzed by PNP Iron Pincer Complexes. *Catal. Sci. Technol.* **2015**, *5* (2), 822−826.
(47) Li, H.; Zheng, B.; Huang, K.-W. A New Class of PN3-Pincer Ligands for Metal-Ligand Cooperative Catalysis. *Coord. Chem. Rev.* **2015**, *293*−*294*, 116−138.
(48) Kalz, K. F.; Brinkmeier, A.; Dechert, S.; Mata, R. A.; Meyer, F. Functional Model for the [Fe] Hydrogenase Inspired by the Frustrated Lewis Pair Concept. *J. Am. Chem. Soc.* **2014**, *136* (47), 16626−16634.
(49) Kubas, G. J. Hydrogen Activation on Organometallic Complexes and H2 Production, Utilization, and Storage for Future Energy. *J. Organomet. Chem.* **2009**, *694* (17), 2648−2653.
(50) Kubas, G. J. Molecular Hydrogen Complexes: Coordination of a. Sigma. Bond to Transition Metals. *Acc. Chem. Res.* **1988**, *21* (3), 120−128.
(51) Kubas, G. J. Fundamentals of H2 Binding and Reactivity on Transition Metals Underlying Hydrogenase Function and H2 Production and Storage. *Chem. Rev.* **2007**, *107* (10), 4152−5205.
(52) Coe, B. J.; Glenwright, S. J. Trans-Effects in Octahedral Transition Metal Complexes. *Coord. Chem. Rev.* **2000**, *203* (1), 5−80.
(53) Satrawala, N.; Sharma, K. N.; Matsinha, L. C.; Maqeda, L.; Siangwata, S.; Smith, G. S.; Joshi, R. K. Base-Catalyzed Cross Coupling of Secondary Alcohols and Aryl-Aldehydes with Concomitant Oxidation of Alcohols to Ketones: An Alternative Route for Synthesis of the Claisen-Schmidt Condensation Products. *Tetrahedron Lett.* **2017**, *58* (28), 2761−2764.
(54) Ouali, A.; Majoral, J.-P.; Caminade, A.-M.; Taillefer, M. NaOH-Promoted Hydrogen Transfer: Does NaOH or Traces of Transition Metals Catalyze the Reaction? *ChemCatChem* **2009**, *1* (4), 504−509.
(55) Clapham, S. E.; Hadzovic, A.; Morris, R. H. Mechanisms of the H2-Hydrogenation and Transfer Hydrogenation of Polar Bonds Catalyzed by Ruthenium Hydride Complexes. *Coord. Chem. Rev.* **2004**, *248* (21−24), 2201−2237.
(56) Wiedner, E. S.; Chambers, M. B.; Pitman, C. L.; Bullock, R. M.; Miller, A. J.; Appel, A. M. Thermodynamic Hydricity of Transition Metal Hydrides. *Chem. Rev.* **2016**, *116* (15), 8655−8692.

https://dx.doi.org/10.1021/acs.inorgchem.9b03476
Inorg. Chem. XXXX, XXX, XXX−XXX